

Imaging with Scattered Neutrons

H. Ballhausen,¹ H. Abele,¹ R. Gähler,² M. Trapp,¹ and A. Van Overberghe²

¹*Institute of Physics, University of Heidelberg, Philosophenweg 12, 69120 Heidelberg, Germany**

²*Institut Laue-Langevin, 6 rue Jules Horowitz BP 156, 38042 Grenoble Cedex 9, France*

We describe a novel experimental technique for neutron imaging with scattered neutrons. These scattered neutrons are of interest for condensed matter physics, because they permit to reveal the local distribution of incoherent and coherent scattering within a sample. In contrast to standard attenuation based imaging, scattered neutron imaging distinguishes between the scattering cross section and the total attenuation cross section including absorption. First successful low-noise millimeter-resolution images by scattered neutron radiography and tomography are presented.

Keywords: scattered, neutron, imaging, radiography, tomography

INTRODUCTION

Conventional neutron imaging [1, 2] always uses a coaxial setup of neutron source, sample and detector (see Fig. 1). The neutron beam is attenuated by absorption and scattering, its shadow being cast on a position sensitive detector behind the sample. The projections obtained in this way are then used to produce radiographs and tomographs. Consequently, these images visualize the total attenuation cross section, the sum of both absorption and scattering cross sections.

The ratio of absorption to scattering varies greatly between different elements. It is therefore crucial to be able to separate the contributions of scattering and absorption or to visualize even coherently scattering inclusions in attenuating bulk material. Many experiments like 3D crystallographic imaging, strain scanning and on hydrogen storage will benefit from and require this basic capability. Scattered neutron radiography has been investigated [3], however, the results were described as preliminary, demanding significant improvements of the technique.

Here, we describe a novel, off-angular setup (see Fig. 2). The detector is set far off the beam axis and views the sample under a significant angle. Only scattered neutrons are detected in this way. Position sensitivity is created by parallel projection using horizontal and vertical collimators between the sample and the detector. These projections made from scattered neutrons can be processed into radiographs and tomographs in the same way as for ordinary neutron or x-ray imaging. However, these pictures only rely on the scattering cross section. Hence, they provide unique and complementary information about the sample.

In this letter we describe the experimental setup, present first radiographs and a tomography. We also discuss possible improvements of the setup and promising perspectives for the technique of scattered neutron imaging.

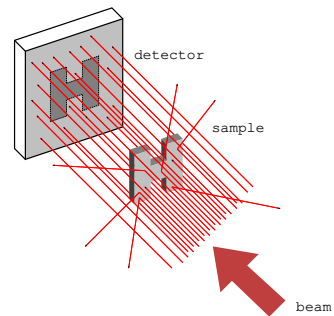


Fig. 1: Conventional neutron imaging: the detector, placed on the beam axis, views the beam attenuated by both absorption and scattering.

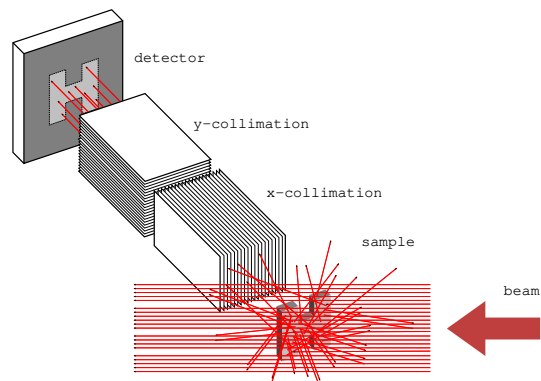


Fig. 2: Scattered neutron imaging: the detector, set far off the beam axis, views the scattered neutrons from the sample via two crossed collimators for position sensitivity.

EXPERIMENTAL SETUP

The experiment is set up at ILL's neutron tomography station [4]. Its beamline H9 delivers a thermal flux of $3 \cdot 10^9 \text{ n cm}^{-2} \text{ s}^{-1}$ at the sample position. Three samples of size $3 \text{ cm} \times 3 \text{ cm} \times 5 \text{ cm}$ are mounted on a motorized slide. They are in the form of the letters C, H and L which stand for carbon (graphite), hydrogen (polyethylene) and lead. The materials were selected because they efficiently scatter neutrons with little absorption:

	$\sigma_{\text{abs.}}$ [barn]	$\sigma_{\text{coh.}}$ [barn]	$\sigma_{\text{inc.}}$ [barn]	$\sigma_{\text{tot.}}$ [barn]	$\mu_{\text{tot.}}$ [cm^{-1}]
hydrogen (PE)	0.333	1.757	80.26	82.35	≈ 7
carbon (graphite)	0.004	5.551	0.001	5.555	0.501
lead	0.171	11.12	0.003	11.29	0.372

Tab. 1: cross sections and attenuation coefficients

The samples are viewed one at a time by two crossed 20' Soller collimators. There is an angle of about 45° between the beam axis and the collimator axis. The collimators are each 40 cm in length, their beam windows are 4 cm wide and divided into 19 slits of each about 2 mm. The collimated neutrons are detected by a LiF-ZnS-scintillator inside an optics housing. The image is projected across two Si-Al-surface mirrors onto a 50 mm $f = 1/1.2$ lens and is recorded by an Andor iXon CCD-camera.

The detection system is optimized for high speed neutron radiography in the millisecond range with good statistics. For scattered neutron radiography, the complete setup is carefully shielded with B_4C rubber mats, the more vulnerable parts with plates of sintered pure $^{10}\text{B}_4\text{C}$. Gamma background is suppressed by clipping greyvalues above a given threshold. Per projection there are 5 to $7.5 \cdot 10^4$ exposures of each 500 ms to acquire sufficient statistics. A reference image acquired without any sample in front of the collimators is subtracted from the data images. No additional digital image filtering is necessary.

EXPERIMENTAL RESULTS

Pyrolytic graphite is well visible in the radiograph (see Fig. 4, left). Its absorption is negligible and it scatters neutrons fairly isotropically due to its polycrystalline structure. The obvious flux reduction on the right side is due to the attenuation of the beam striking the sample from the left side.

This effect is even more pronounced for hydrogen (see Fig. 4, right), because its total attenuation coefficient $\mu \approx 7 \text{ cm}^{-1}$ is about fourteen times higher than for graphite. Consequently, the signal decreases already in the left bar of the letter 'H', which is one centimeter thick, from left to right; the signal increases in the middle of this bar due to multiple scattering from below and above; and there is a faint signal on the left side of the right bar, because the front part of this bar is partly exposed to the unattenuated beam due to the 45° orientation of the sample.

In both images the pixelation due to the collimators is visible. It is more pronounced horizontally than vertically as the y -collimator is directly in front of the scintillator. The vertical boundaries are blurred due to the distance to the x -collimator by about the size of a pixel, 2 mm, defining the limit of spatial resolution. The faint bar beneath all letters is that part of the aluminium sample holder which is within the $4 \text{ cm} \times 4 \text{ cm}$ field of view.

Lead is a purely coherent scatterer. The fact that the letter 'L' is still visible in a scattered neutron radiography (see Fig. 5, left) is proof of the fact that standard lead is a polycrystall. However, there are several especially dark spots in the image. At first sight, they could be small yet strong scatterers embodied in the bulk material.

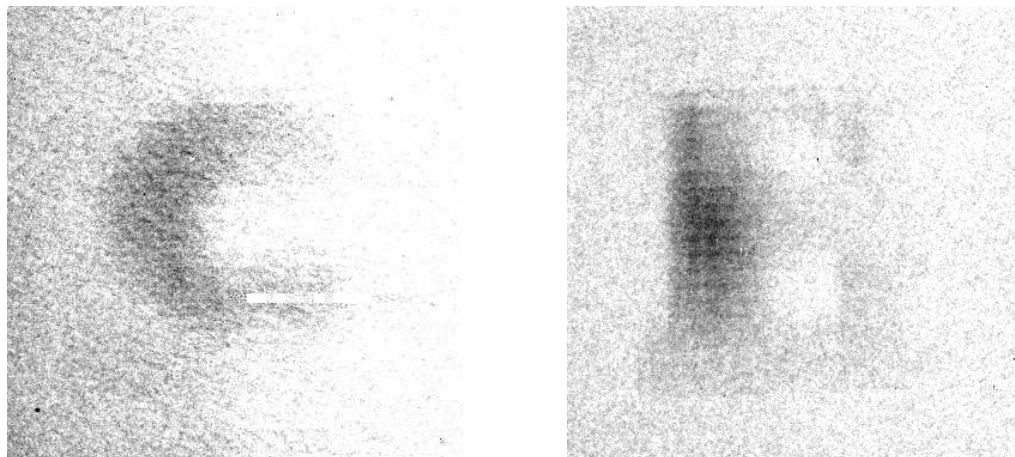


Fig. 4: scattered neutron radiographies of graphite and polyethylene

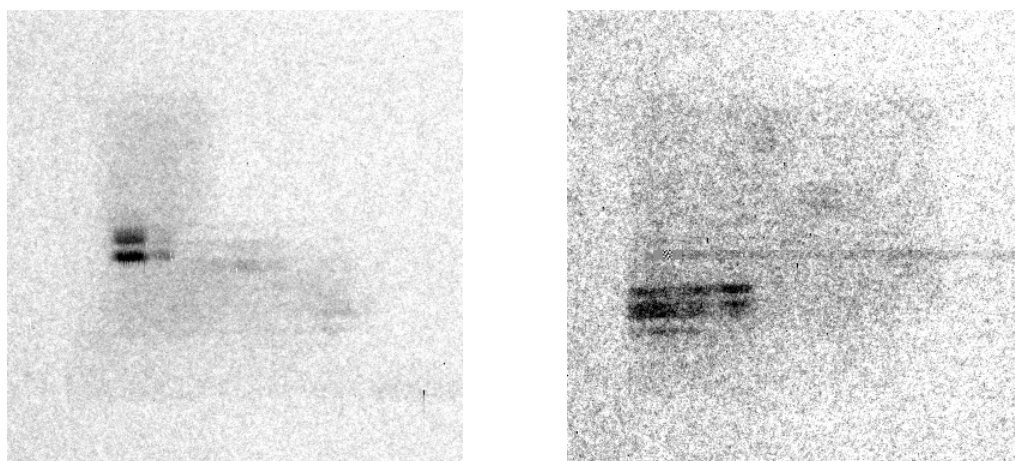


Fig. 5: (partly coherently) scattered neutron radiographies of lead

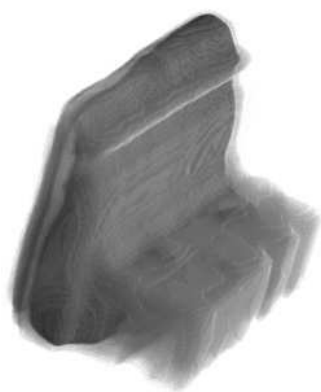


Fig. 6: scattered neutron tomography of the lead sample

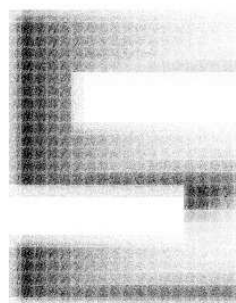


Fig. 7: Monte Carlo simulation displaying effects of self-attenuation

To check this hypothesis the sample was turned by 90° relative to the detector. The image, now showing the back of the letter 'L' (see Fig. 5, right), was combined from two exposures for a larger field of view. Again, there appear peaks in the signal. This time, however, they show up at a different height in the sample and can thus not originate from the same region in the sample. The conclusion is that the peaks in the signal are produced by small coherently scattering crystals orientated by chance to fulfill the Bragg condition in direction of the detector. When the sample is rotated, different scattering centers flash up at different orientations.

Several exposures of the same image, for example of the letter 'L', can be processed into a scattered neutron tomography of the sample (see Fig. 6). Especially for this purpose, the effects of coherent scattering and self-attenuation within the sample, need to be taken into account in the future. To study these effects systematically, Monte Carlo simulations are being developed (see Fig. 7).

CONCLUSION AND OUTLOOK

Images by scattered neutron radiography and tomography are presented. Both incoherent (H) and coherent scatterers (C, Pb), and even weak scatterers (Al) are visualized with millimeter resolution. It is worthwhile to consider possible improvements of the method:

Using crossed collimators, the resolution is limited by the width of the slits. Here flux can be gained by making the collimators just shorter, without any loss of position sensitivity. With collimators of 4 cm in length instead of 40 cm, a factor of 100 in flux can be gained. The limit is the size of the sample, which should be smaller than the collimators because of the blurring of the projection. A real improvement is a honeycomb collimator which combines x - and y -collimation on the same length as a Soller collimator, doubling resolution and quadrupling flux.

In contrast to ordinary neutron imaging, image quality and resolution are not dependent on the collimation of the incoming beam. This is a strong point in favour of high-flux medium-collimation installations like at ILL. It would be possible to set up an instrument dedicated to scattered neutron imaging very close to a reactor core or a spallation target, for example at an existing irradiation facility. Also, several detector patches can be positioned around the sample forming an effective 4π -detector.

Scattered neutron imaging adds another geometrical degree of freedom to neutron imaging. Coherently scattering domains will lighten up under Bragg angles, so their three dimensional distribution and orientation in the sample can be determined for 3D-crystallography. On the other hand, and more fundamentally, scattered neutron imaging adds two spatial degrees of freedom to general neutron spectrometry, diffractometry, etc. In principle, regardless of flux and resolution, the hallmark experiments of neutron science could broaden their horizon from small homogenous samples to structured heterogenous objects.

* Electronic address: ballhausen@physi.uni-heidelberg.de

- [1] H. Kallmann:
Neutron Radiography
Research 1 (1948) 254-260
- [2] T. J. Bücherl (ed.):
Proc. 5th International Topical Meeting on Neutron Radiography
Elsevier 2004
- [3] H. Kobayashi, M. Satoh, K.-Y. Nam:
Preliminary Study for an Imaging Technique Using Scattered Radiations
Proceedings of the Seventh World Conference on Neutron Radiography 2002
in: IEEE Transactions on Nuclear Science, Vol. 52, No. 1 (2005) 375-379
- [4] The neutron tomography station at ILL is a joint test experiment run in collaboration between the Institut Laue-Langevin and the University of Heidelberg. It has been funded by the German Federal Ministry for Research and Education under contract number 06HD153I.